



Process optimization of a closed-chamber distillation system for the recovery of FLiNaK molten salt

Jun-Xia Geng^{1,2} · Yang Yang¹ · Hai-Ying Fu^{1,2} · Yan Luo^{1,2} · Qiang Dou^{1,2} · Qing-Nuan Li^{1,2}

Received: 11 September 2020 / Revised: 16 November 2020 / Accepted: 21 November 2020 / Published online: 19 January 2021
© China Science Publishing & Media Ltd. (Science Press), Shanghai Institute of Applied Physics, the Chinese Academy of Sciences, Chinese Nuclear Society 2021

Abstract Low-pressure distillation has been proposed as a suitable technique for the recovery of carrier salt from molten salt reactor spent fuel. A closed-chamber distillation system, in which the pump is stopped and pressure-induced salt distillation is performed, was arranged for fluoride salt treatment. A stair-step optimization process was demonstrated to improve the recovery efficiency by up to 99%. The pressure change curve was feasible for estimating the distillation process, and a method for displaying the pressure value online in order to determine the endpoint was also developed. The decontamination factor of Nd in the condensate salt was deduced to be greater than 100 with 1 wt% NdF₃-FLiNaK distillation. The optimal conditions developed in this study showed a high recovery ratio for the fluoride carrier salt and a high separation efficiency for rare earth products.

Keywords Low-pressure distillation · Closed chamber · Fluoride molten salt · Recovery ratio

This work was financially supported by the National Natural Science Foundation of China (No. 21771188) and the Strategic Priority Research Program of the Chinese Academy of Sciences (No. XDA02030000). A study on some key issues regarding the Th-U fuel cycle was also funded (No. QYZDY-SSW-JSC016).

✉ Hai-Ying Fu
fuhaiying@sinap.ac.cn

✉ Qiang Dou
douqiang@sinap.ac.cn

¹ Shanghai Institute of Applied Physics, Chinese Academy of Sciences, Shanghai 201800, China

² University of Chinese Academy of Sciences, Beijing 100049, China

1 Introduction

Compared with aqueous media, molten salts (mainly fluorides, chlorides, and nitrates) have many advantages, such as low vapor pressure and high heat capacity. Therefore, molten salts have been applied in many fields, such as extraction, high-temperature electrolysis, thermal energy storage, and heat transfer media [1–4]. In nuclear power systems, molten salts are typically used as the coolant for molten salt reactors (MSRs) and electrolyte for electrochemical separation in spent nuclear fuel reprocessing. For example, molten LiF-BeF₂-ThF₄-UF₄ was selected as the fuel carrier salt and coolant of a molten salt breeder reactor (MSBR), which was developed and tested at the Oak Ridge National Laboratory (ORNL) [5].

One of the characteristics of MSRs is that the fuel is dissolved in a molten carrier salt; therefore, after a period of operation, the spent nuclear fuel of the MSR contains ⁷LiF-BeF₂ carrier salts, uranium, thorium, and fission products (FPs). For waste minimization and reactor economy improvement, it is necessary to separate the FPs from the carrier salt and recover the useful components, such as uranium and plutonium, especially high-cost and high-purity ⁷LiF. Because the volatilities of most FPs, such as rare earths and alkaline earth fluorides, are significantly lower than that of LiF, the low-pressure distillation technique, which is based on the vapor pressure difference, shows potential application in carrier salt recovery and FP removal. Considering the principle of low-pressure distillation, separation can usually be achieved without adding other reactants; thus, fewer by-products are formed during distillation [6], further reducing the volume of waste involved.

To date, many research groups have focused on the utilization of low-pressure distillation for salt recovery in the nuclear field. As early as the 1960s, ORNL began to investigate the relative volatilities of fission-produced fluorides using an equilibrium distillation apparatus; on this basis, one engineer-scale demonstration was carried out to demonstrate the feasibility of using a low-pressure distillation method to recover carrier salts [7, 8]. In addition, a conceptual design of a fluorination–vacuum–distillation system, in which the fluorination of uranium and low-pressure distillation could be carried out continuously, was proposed [9]. However, the development of fluoride distillation was suspended owing to the termination of the molten salt reactor experiment (MSRE) in the 1970s. Recently, several concepts for MSR have been developed owing to the advantages of molten salts. Chloride salts were used as carrier salts in fast-neutron reactors, owing to the low fast-neutron cross section of Cl. Similar to other nuclear reactors, relative reprocessing technology has also been explored to recover useful materials and reduce the volume of waste, including techniques such as chloride molten salt electrochemistry, ion exchange, and distillation. For example, to recover uranium and separate FPs, the Korea Atomic Energy Research Institute (KAERI) has developed electrochemical reduction and electrochemical refining technologies, in which molten chloride salts (LiCl–KCl, NaCl–KCl, or NaCl–Li₂O) are used as electrolytes in electrochemical processing.

Low-pressure distillation techniques have also been developed to manage some of the electrolyte salts adhered to the electrorefining products at Idaho National Laboratory (INL) [10, 11], KAERI [12–14], and the Central Research Institute Power Industry (CRIEPI) of Japan [15]. At INL, the liquid cadmium cathode and chloride salts were evaporated individually by controlling the system at reasonable temperatures. At KAERI, the distillation behavior of chloride salts (LiCl, KCl, or their mixture) was studied at different experimental scales, and distillation was improved with reagents, such as rare earth oxychlorides or oxides that are less soluble in salt and have greater pressure differences with salts that were preformed by adding oxygen, H₂O, or oxides before chloride salt distillation. These evaporation processes occurred on heterogeneous surfaces between the liquid and liquid phase or liquid and solid phases, which made achieving an ideal separation effect more beneficial.

Compared with chloride salts, fluoride salts have higher melting points and lower vapor pressures and are more corrosive, which brings more challenges [16, 17]. One of these is the increased difficulty for the apparatus to achieve distillation separation, requiring a higher evaporation temperature, better sealing performance, and stronger corrosion resistance. Meanwhile, because of the higher

melting points, the vapor of the fluoride salts condenses in undesirable locations, such as the dead ends of tubes or exteriors of collection containers, ultimately reducing the distillation recovery ratio and exposing the equipment to the risk of secondary contamination.

The staff at the Shanghai Institute of Applied Physics have been developing a thorium MSR (TMSR) since 2011. To reprocess TMSR nuclear fuel, a preliminary conceptual design is determined to remove FPs and fissile materials from these fused fluoride mixtures. First, the salt comes into contact with fluorine gas, resulting in the removal of uranium as volatile UF₆. The off-gas product also contains certain volatile fluoride FPs, such as molybdenum, ruthenium, and technetium. Then, the salt is fed to a low-pressure still, where the carrier salts LiF and BeF₂ are vaporized and recovered, while fluoride FPs that are less volatile than LiF remain in the still and are discarded. Some relevant work has been carried out in the last 10 years [18–22]. Based on the requirement of the disposal or processing of spent fuel salts of TMSRs, our group has focused on investigating the distillation behavior of FLiNaK molten salt and the removal efficiency of some typical rare earth fluorides (REFs) in a FLiNaK system using an alundum furnace [22]. It was found that some condensate entered the filter with the pump running, which reduced the recovery ratio.

In the present work, a closed-chamber distillation system with a single sealing flange and independent three-zone temperature controllers was established to improve the recovery ratio. A feature of this distillation system is that the vacuum pump was turned off during the distillation process, and the temperature gradient of the chamber directly affected the pressure difference between the evaporation and condensation zones. We applied FLUENT software to analyze the temperature distribution of this closed-chamber distillation system and optimized the process conditions (mainly the setting of temperature and vacuum) suitable for distilling the fluoride molten salt. The FLiNaK eutectic melt was used as the simulated salt because its melting point was similar to that of the coolant salt FLiBe in the MSR. The relationship between the recovery ratio and distillation temperature is also discussed. Under the optimized conditions, the separation degree achieved with 1 wt% NdF₃–FLiNaK was further evaluated.

2 Materials and methods

2.1 Reagents and materials

High-grade anhydrous fluorides (LiF, NaF, and KF; > 99.95%) and NdF₃ (> 99.99%) were purchased from

Sigma-Aldrich Co., Ltd. All other reagents were of analytical grade and were used without further purification.

The compositions of the FLiNaK eutectic system were 46.5 mol % LiF, 11.5 mol % NaF, and 42.0 mol % KF. FLiNaK was obtained according to the literature [23].

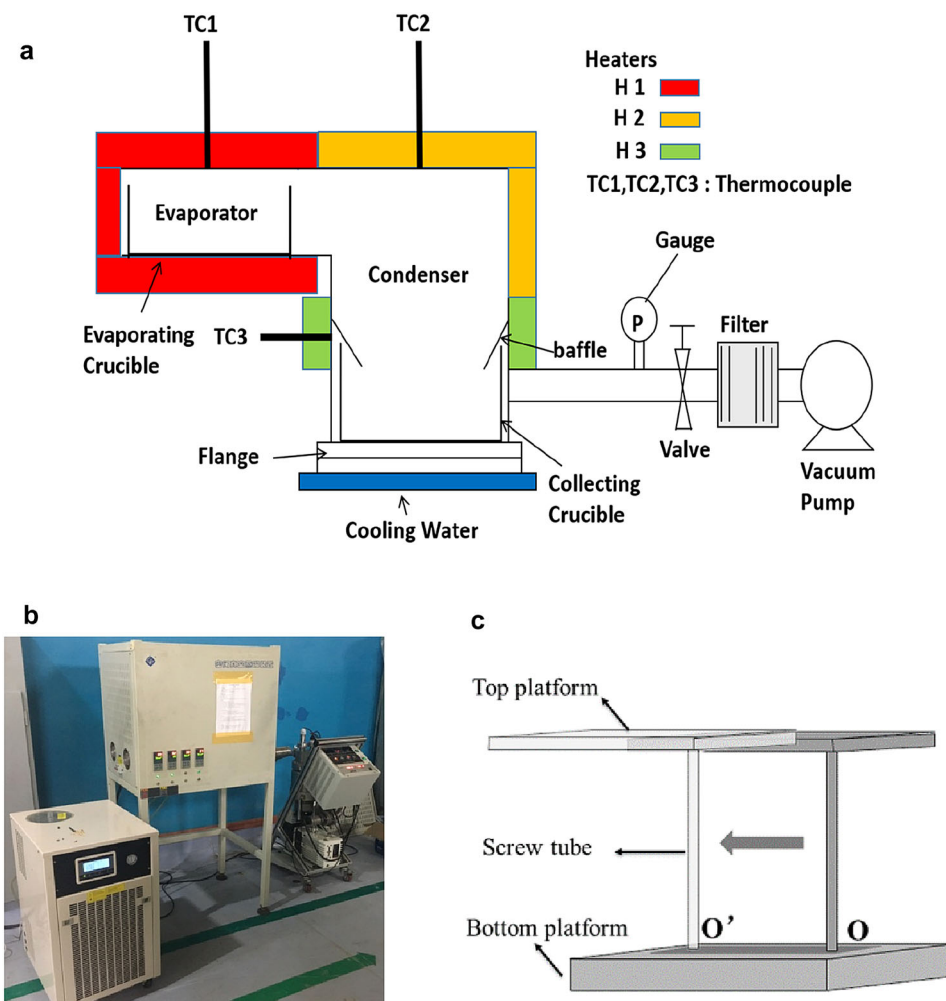
2.2 Experimental setup

A schematic illustration of the distillation system is shown in Fig. 1a. This system mainly consisted of a furnace, two chambers, cooling water, and vacuum systems as shown in Fig. 1b. The two adjacent chambers were used for evaporation and condensation. The left evaporation chamber with a diameter of 120 mm and height of 120 mm was directly connected to the right condensation chamber with a diameter of 200 mm and height of 440 mm. Both chambers, made of stainless steel (SUS-310S), were designed to be heated by three heaters: H1, H2, and H3. The maximum temperature is as high as 1200 °C for H1 and H2 and 800 °C for H3. In the system, three thermocouples were installed in the middle of the individual

heater, denoted as TC1, TC2, and TC3. Refrigerated water was used to cool the bottom flange. The vacuum system was composed of a mechanical pump (Edwards RV 12) and a molecular pump (KYKY FF-160/620), which can achieve a pressure of 10^{-3} Pa. The former pump worked first; then, the latter began to run when the pressure decreased to 100 Pa. A vacuum gauge was installed in front of the valve to display the pressure value online.

A special bracket, which was made of stainless steel (SUS-304), was devised to load and unload the evaporation crucible, as shown in Fig. 1c. The screw tube, connected to the top and bottom platforms, was adjustable. First, the screw tube was fixed at location O, and the evaporation crucible was placed on the top platform of the bracket. Then, the bracket was elevated until the top reached the height of the evaporation chamber. Second, the screw tube was moved to location O', according to the groove on the bottom platform, and was moved to the evaporating crucible to the center of the evaporation chamber. Finally, the bracket was removed from the chamber.

Fig. 1 (Color online) (a) Scheme of the closed-chamber distillation system, (b) photograph of the closed-chamber distillation system, and (c) scheme of the sample bracket



2.3 Melt preparation

A furnace was placed inside a glove box in an argon atmosphere, wherein the H₂O and oxygen contents were controlled below 1 ppm. Certain amounts of pretreated fluorides, LiF, NaF, and KF, were mixed in a nickel crucible, which was placed inside the furnace. The furnace was first heated to 300 °C and maintained for 1 h to remove trace moisture. Then, the temperature was raised to 650 °C, where it was maintained for 5 h until the fluorides completely melted. The prepared melt was slowly cooled to the ambient temperature.

The salt mixture containing 1.0 wt% NdF₃, denoted as NdF₃-FLiNaK, was prepared by a similar treatment. A more detailed description was reported in our previous study [22].

2.4 Distillation

Approximately 200 g of FLiNaK salt or NdF₃-FLiNaK salt was placed in an evaporation crucible with a diameter of 100 mm. Then, the crucible was placed on top of the bracket and transported to the evaporator chamber. The collection crucible located on the bottom of the condenser was raised to the distillation chamber flange, and the entire chamber was closed. Next, the pressure of the chamber was reduced to 100 Pa, using a mechanical vacuum pump, and the molecular pump was operated to further reduce the pressure to 10⁻³ Pa. Then, the three heaters were turned on to heat the chamber to the given temperatures. When the temperature reached the given temperature, the two pumps were stopped, and distillation was carried out. The changes in temperature and pressure were recorded. After the end of distillation, the heaters were turned off to cool to 20 °C; then, the pressure inside the distillation system was restored. Finally, the evaporation crucible and collection crucible were removed and weighed.

2.5 Measurement and chemical analysis

The recovery and evaporation ratios were used to evaluate the recovery and evaporation efficiencies. The average value obtained with three repeated experiments was given, with a relative error of less than 10%.

The salt recovery ratio was defined as the ratio of the mass of the collected salt to that of the evaporated salt and can be calculated using Eq. (1):

$$\text{Recovery ratio} = \frac{M_C}{M_0 - M_L} \times 100\%. \quad (1)$$

M_0 , M_C , and M_L correspond to the masses of the original salt to be distilled, condensed salt collected in the

collection crucible, and residual salt in the evaporating crucible, respectively.

The evaporation ratio was defined as the ratio of the mass of the evaporated salt to that of the original salt and can be calculated using Eq. (2):

$$\text{Evaporation ratio} = \frac{M_0 - M_L}{M_0} \times 100\%. \quad (2)$$

The decontamination factor, abbreviated as DF , was used to evaluate the separation efficiency of rare earth elements from the carrier salt, which was represented by the mass fraction ratio of the analyzed element in the original salt to the condensate salt and was defined as

$$DF = \frac{M_{R0}/M_0}{M_{RC}/M_C}, \quad (3)$$

where M_{R0} and M_{RC} correspond to the masses of the REFs in the original salt and condensate salt, respectively.

The composition of the salt sample was analyzed by inductively coupled plasma optical emission spectrometry (ICP-OES), according to a method presented in a previous work [22]. Each sample was analyzed three times, and the relative error of the parallel samples was below 5%.

3 Results and discussion

3.1 Sealability determination

In contrast to the equipment used in KAERI [24], the closed-chamber distillation system has only one flange located at the bottom of the condenser, which is used to load the salt and seal the chamber. The other parts of the body are welded together, and the top is flat, which makes the system simpler and easier to fabricate and install. Because there is only one open flange, the sealing performance of the equipment is theoretically further improved, and the molten salt vapor can be prevented from escaping from the distillation chamber with a certain probability.

To test the gas tightness of the chamber, the change in the gas pressure of the blank chamber was measured, and the measured pressure was used as the background pressure of this chamber. The leak rate was measured using a helium leak detector, yielding a value of less than 10⁻⁷ Pa m³/s. After the bottom flange was sealed, the vacuum pressure was evacuated to approximately 0.1 Pa by the vacuum system. Then, the entire chamber was heated to approximately 500 °C at 10 °C/min and maintained at 500 °C for 20 min. The pump continued to operate during heating and holding. When the left side of the distillation chamber was heated to approximately 1000 °C (H1) at 10 °C/min and H2 and H3 were increased to 600 °C, the vacuum pumps were stopped, and the system was finally

sealed. The pressure change curve was recorded, as shown in Fig. 2ii. The pressure of this system increased very slowly, including the 4 h when the temperature of the system was maintained at 1000 °C and the pressure was maintained at 10 Pa. The background pressure increasing rate was deduced to be less than 0.05 Pa/min. This value was significantly lower than the vapor pressure of the FLiNaK or FLiBe salt at the same temperature [25]. In general, for no-carrier distillation, the vapor pressure of the salt must be significantly higher than the background gas pressure [26] to allow for sufficient effective evaporation. Hence, this system was deemed feasible for treating species with low vapor pressure because of the sufficiently low vacuum pressure of the chamber.

3.2 Temperature gradient simulation

Generally, the temperature gradient in the distillation chamber is another very significant driving force for salt evaporation and condensation, significantly affecting the rate of distillation and adhesion of the condensate. The temperature distributions in the closed-chamber system were calculated by using the computational fluid dynamics (CFD) method with FLUENT software, as described in References [27, 28].

In the present work, computational software was used to simulate the temperature distributions with different temperature settings. The temperature calculation performed inside the entire chamber with the heaters is shown in Fig. 3.

According to our previous work [22], the evaporation temperature of the fluoride salt was greater than 900 °C, and the evaporation rate could increase at a higher temperature. ORNL also investigated the relative volatility of

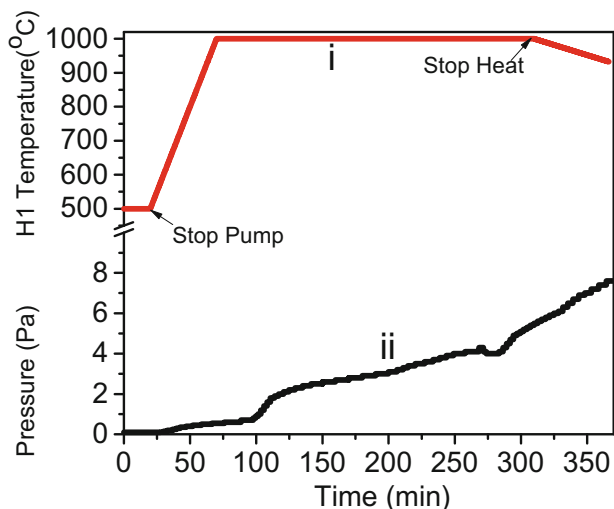


Fig. 2 (Color online) Background gas pressure at high temperature. (i) Temperature curve; (ii) pressure curve

REFs in the FLiBe system at approximately 1000 °C [6]. Based on this, in the calculation of the temperature field distribution in this study, the temperature of the evaporation area was directly set to 1000 °C.

Meanwhile, as the H1 temperature was set to 1000 °C and the H2 and H3 temperatures ranged from 900 to 550 °C (denoted as 1000–900–550 °C), the actual temperature inside the chamber was measured by temperature control blocks (Type L1 or L2, Japan Fine Ceramics Center). One block was placed in a crucible at point T1, which was also the center point of the evaporation crucible. The other block was fixed on a special stage that was at the same height as point T2, as shown in Fig. 3i.

As shown in Fig. 4, the difference between the simulated data and measurement was less than 30 °C; hence, it was useful to set up the experiment using temperature simulation. Furthermore, considering the temperature between T1 of the evaporator center and T2 of the condenser for the three conditions, the temperature gradient inside the chamber could be adjusted by changing the H2 and H3 temperatures.

3.3 Distillation condition optimization

Based on the simulation temperature distribution results, three distillation experiments, namely Runs 1–3, were performed for 200 g FLiNaK melts. Crude salt, which was slightly gray, was loaded in a nickel crucible with a diameter of 100 mm and placed in the evaporator chamber; then, the crucible was fixed to the evaporation zone using the bracket. The collection crucible was located on the bottom flange of the condenser.

Table 1 shows the evaporation ratio and recovery ratio under different conditions. The recovery ratios of the three runs (Runs 1–3) were all no greater than 90%. In Runs 1 and 2, a portion of the salt was observed to attach to the inner wall, especially on the baffle, as shown in Fig. 5a, which may result from the low temperature of the condenser. Compared with that of Run 1, the recovery efficiency of Run 2 was better. In Run 3, only 91.4% of the salt was evaporated with the same distillation time. A possible reason may be the narrower temperature gradient between H1 and H2, as shown in Fig. 3iii, which might prevent vapor flow from the evaporator to the condenser. These results showed that relatively low condenser temperatures accelerated salt distillation but reduced the recovery ratio. The recovery ratio was less than 99%, and more than 1% salt was condensed and released from the receiver, which may have solidified on some inner wall or baffle. According to the temperature gradient simulation and experimental results of Runs 1–3, it was possible to change the temperature of the H2 and H3 zones to improve the recovery efficiency. Therefore, the temperatures of the H2

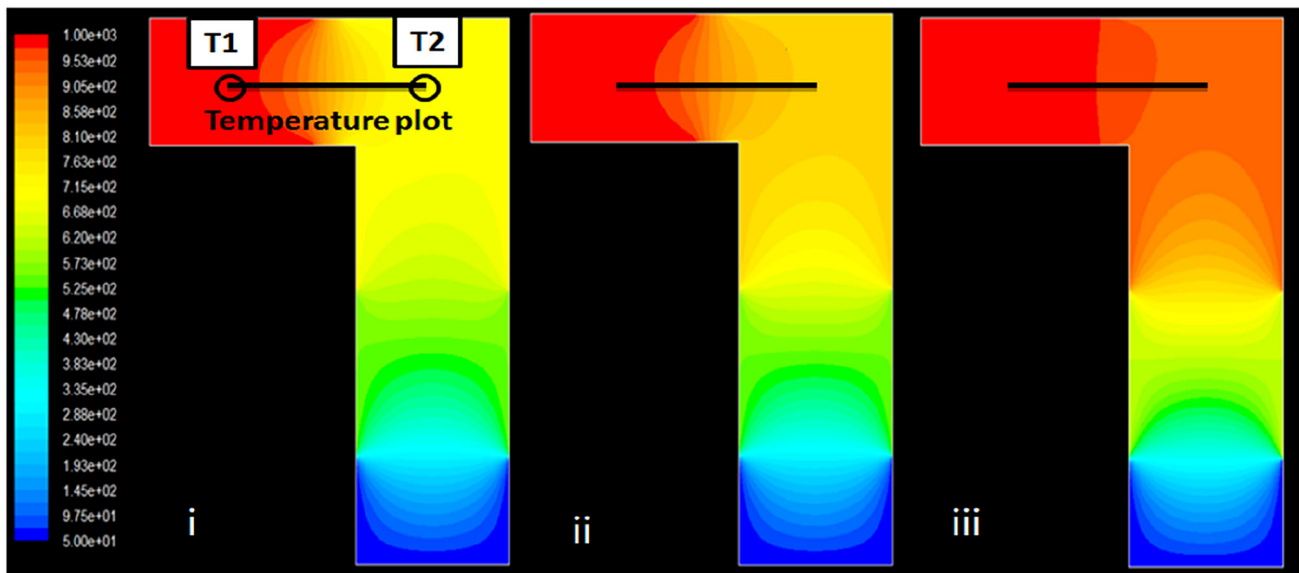


Fig. 3 (Color online) Temperature calculated inside the whole chamber with the heaters: (i) 1000–700–550 °C, (ii) 1000–800–550 °C, and (iii) 1000–900–650 °C

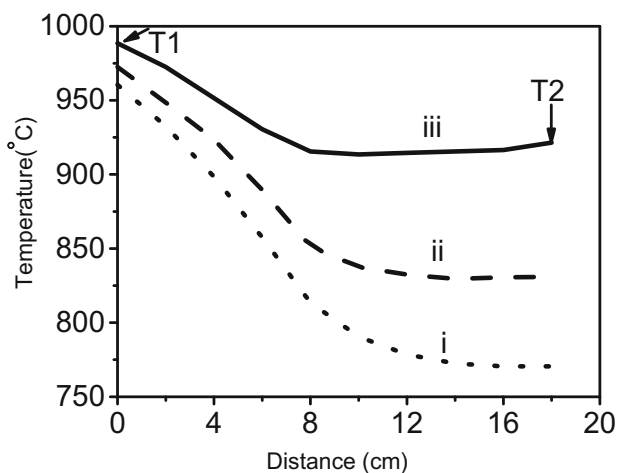


Fig. 4 Temperature change curve between T_1 and T_2 for (i) 1000–700–550 °C, (ii) 1000–800–550 °C, and (iii) 1000–900–650 °C

and H3 zones were adjusted to reduce the amount of salt solidified on some inner walls and improve both the evaporation and recovery ratios. Therefore, the sectional heating of H2 and H3 was carried out by stair-step heating.

For example, in Run 4, a typical stair-step heating method was adopted, in which the evaporation temperature (H1) was set to 1000 °C throughout. However, H2 was set to 700 °C in the first 2 h; then, it was increased to 900 °C in 1 h and maintained at 900 °C until the experiment was completed. Similarly, the temperature of H3 was maintained at 500 °C in the first 2 h, raised to 650 °C in 1 h, and maintained until the end. After 4 h of distillation, almost 100% of the salt was evaporated, and the recovery ratio of FLiNaK reached 99.4%. Furthermore, the condensate salt was collected in the collector, as shown in Fig. 5c, and no salt was observed on the inner wall of the chamber, as shown in Fig. 5b. In this case, the recovery

Table 1 Evaporation and recovery ratios obtained under different working conditions

Run	Distillation time (h)	H1 (°C)	H2 (°C)	H3 (°C)	Evaporation ratio (%)	Recovery ratio (%)	
1	4	1000	700	550	99.6	86.6	
2	4	1000	800	550	97.2	90.4	
3	4	1000	900	650	91.4	82.3	
4	4	2	1000	700	550	99.9	99.4
		1	1000	700–900	550–650		
		1	1000	900	650		

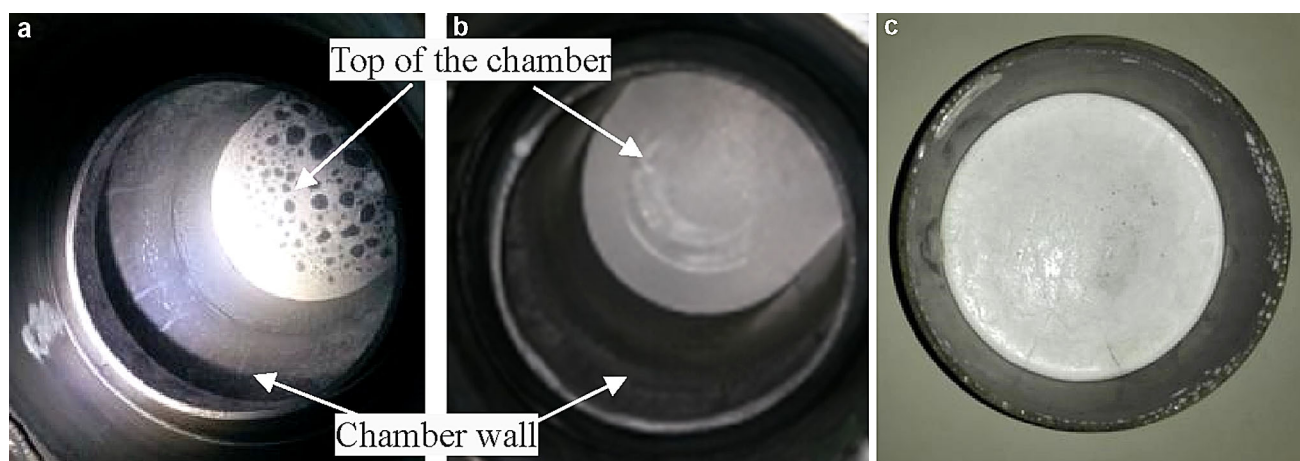


Fig. 5 Photographs of the inner chamber after distillation: (a) Run 1, (b) Run 4, and (c) condensate salt

efficiency was enhanced. Therefore, the stair-step method could improve the distillation efficiency. Furthermore, the salt collected in the receiver was white, and the corrosion products Fe, Ni, or Cr from the SUS 310S chamber were difficult to measure by inductively coupled plasma optical mass spectrometry (ICP-MS) analysis. Additionally, after distillation, the inner wall of the chamber was smooth. These results indicated that the condensate salt was of high quality and that the corrosion of the salt could be neglected.

The experimental phenomena observed were consistent with the physical characteristics of the condensate salt. The temperature of the condenser was critical to maintaining the salt liquidus. In ORNL, FLiBe–ZrF₄ carrier salts of the MSRE were demonstrated to be condensed in the temperature range of 550–700 °C, and the vapor stream containing greater than 90 mol % LiF required higher condenser temperatures of approximately 800–900 °C [25]. Therefore, the temperature of the zone between the evaporation crucible and receiver for Runs 1–3 was low, while LiF or NaF with low volatilities tended to condense at 550–600 °C before entering the receiver. However, in stair-step heating (Run 4), with the reheating of H₂ and H₃ in the distillation process, the temperature of the inner wall increases again, and the salt that is first attached to the inner wall of the chamber might melt and flow into the receiver. Hence, the recovery efficiency of the distilled salt was improved by using the stair-step heating mode.

Furthermore, a higher recovery ratio indicates less salt loss. In addition, owing to the shutting off of the pumps, the distillation process was carried out in a nearly closed environment, which made it impossible for the material to be distilled and released from the apparatus. Therefore, this distillation mode showed potential for preventing radioactive leakage.

3.4 Pressure change analysis

For a distillation system, it is important to determine the distillation process to facilitate the determination of whether the system runs well or needs to be shut down. For instance, in our previous research, the beginning and end of the distillation process could be determined via the balance located on top of the distillation chamber [26]. However, this method does not apply to closed-chamber distillation. The pressure change curve may offer a method to confirm the distillation process. In this distillation equipment, a resistance vacuum gauge was installed next to the chamber valve for system pressure monitoring, as shown in Fig. 1. The pressure value was recorded online, which reflected the change in the chamber pressure. The salt distillation process was assumed as in the literature [29], according to the change curve.

The pressure changes of Runs 5–8 were operated under the same distillation conditions as those of Run 4; however, different salt amounts were used, as shown in Fig. 6. Using

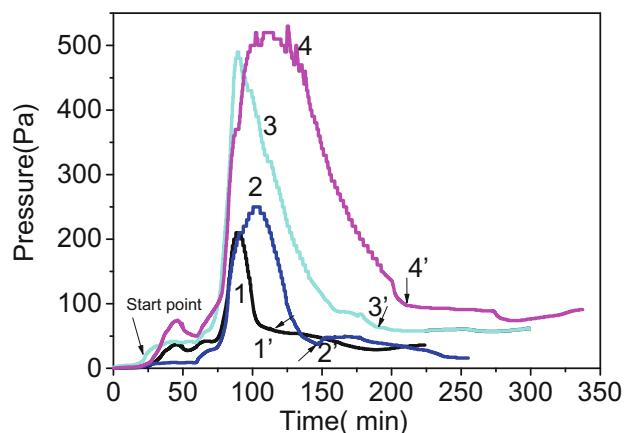


Fig. 6 (Color online) Pressure change curves of the distillation of (1) 100 g, (2) 200 g, (3) 300 g, and (4) 400 g of FLiNaK

curve c in Fig. 6 as an example, 300 g of FLiNaK was distilled under the conditions of Run 7, and the pressure was recorded. When the temperature of the chamber reached 500 °C, the pumps were turned off, and this moment was recorded as 0. First, the pressure of the entire chamber was less than 0.1 Pa. As the temperature increased, the pressure increased gradually. Over the next 25 min, as the temperature increased to 750 °C, the pressure increased considerably, suggesting that some evaporation had occurred. Then, another peak was observed at the constant temperature zone, and the maximum pressure reached approximately 500 Pa. Afterward, the pressure was reduced to a relatively constant value. As shown in Fig. 6, the same pressure tendency could be obtained using different amounts of molten salt. When the pressure value was constant, the furnace was shut off, and little salt was found remaining in the evaporation crucible, indicating that the distillation of the salt had terminated. Based on this, the time when the pressure curve started to show a constant value was considered the end of the distillation process. For example, distillation was regarded as ending at points 1', 2', 3', and 4', corresponding to 115, 145, 186, and 218 min, respectively, after the pump was turned off. The pressure began to increase at 25 min, which corresponds to the starting point of the distillation process.

According to the pressure curve, the distillation rate of FLiNaK was further derived using Eq. (4):

$$V = \frac{M_C - M_L}{S \times t}, \quad (4)$$

where V is the distillation rate in $\text{g}\cdot\text{cm}^2\text{min}^{-1}$, S is the evaporation surface area in cm^2 , and t is the time of distillation in min, which is determined by the difference between the start and end points.

The results are listed in Table 2. For this system, the FLiNaK distillation rate for Runs 5–8 ranged from 0.015 to 0.027 $\text{g}\cdot\text{cm}^2\text{min}^{-1}$, which indicates that the method for determining the distillation time based on the pressure curve was reliable. Compared with the distillation rate for a continuously operating vacuum pump [22], the distillation rate in this study was slightly lower. Here, the error of the distillation rate was introduced by the error in determining the distillation endpoint; thus, a more precise and sensitive pressure sensor can further improve the accuracy of the distillation rate. In the following separation experiment of

Table 2 Distillation rate of FLiNaK melts

	Run 5	Run 6	Run 7	Run 8
Salt (g)	100	200	300	400
V ($\text{g}\text{cm}^{-2}\text{min}^{-1}$)	0.015	0.020	0.023	0.027

NdF₃–FLiNaK, the method of pressure change was used to detect the distillation process.

3.5 Decontamination factor of Nd

The ultimate aim of the salt distillation process developed in the TMSR is to separate the FPs, especially REFs, and eventually recover the purified fluoride molten salt. Therefore, the separation efficiency of REFs is one of the key specification targets of distillation treatment. The decontamination factor (DF) was used to evaluate the separation efficiency.

FLiNaK salts (200 g) containing 1.0 wt% NdF₃ were distilled using the same stair-step temperature mode as Run 4. With evaporation ratios ranging from 27 to 99%, the DF s of Nd are listed in Table 3. The results showed that the DF of Nd reached 10^2 , which is satisfactory for the purification of a fuel carrier salt using distillation technology. In addition, the REF DF s decreased with an increase in the evaporation ratio because NdF₃ could be dissolved in the carrier salt, and during the process of distillation, the concentration of NdF₃ increased with increasing evaporation ratio, which led to concentration polarization and contamination of the condensate salt. For example, with a 27% evaporation ratio, the content of Nd in the condensate was measured to be 9.3 ppm, and the DF value was deduced to be 1.08×10^3 . For a 99% evaporation ratio, the content of Nd was approximately 75 ppm, and the DF value was 1.3×10^2 .

Table 3 also shows that the main composition of the condensed salt varied at different evaporation ratios, which indicated that the ratio of the evaporation rate was not consistent with the molar ratio of each component. The volatilities and evaporation rates of the LiF, NaF, and KF components in the FLiNaK carrier salt were different, and the three fluorides retained their own chemical species; thus, it was assumed that LiF, NaF, and KF could be evaporated separately but not simultaneously.

Therefore, according to the Hertz–Langmuir equation [29], the evaporation rate is proportional to the partial pressure, which can be derived as Eq. (5):

$$V_{\text{net}} = \frac{\alpha P}{\sqrt{2\pi RT/M}}, \quad (5)$$

where V is the net evaporation rate, $\text{g}\cdot\text{cm}^{-2}\text{min}^{-1}$, R is the gas constant, and T is the temperature, K. Additionally, M is the molecular weight, P is the partial pressure, Pa, and α is the evaporation coefficient. Parameter α is determined by the molecular interactions at the evaporation surface. For the FLiNaK salt, the LiF, NaF, and KF vapors interacted with each other on the same surface; thus, α was assumed to be the same. According to the literature [30], the ratio of the partial pressures of each component in the

Table 3 Compositions and decontamination factors of Nd in salt condensed at different evaporation ratios

	Run 9	Run 10	Run 11	Run 12
Duration time/ min	1000–700–550 °C 10 min	1000–700–550 °C 30 min	1000–700–550 °C 1 h	1000–700–550 °C 2 h 1000–950–650 °C 2 h
	1000–950–650 °C 10 min	1000–950–650 °C 30 min	1000–950–650 °C 1 h	
Evaporation ratio	27%	44%	74%	99%
DF of Nd	1.08×10^3	3.4×10^2	2.6×10^2	1.3×10^2
LiF mol%	10	23.4	35	45
NaF mol%	2.8	4.6	5.5	12.2
KF mol%	87.2	72	60	42.8

FLiNaK salt was derived, with the partial pressure ratios of LiF/NaF/KF in the FLiNaK salt deduced to be approximately 1:1.5:10 at 1000 °C. This corresponds to a ratio for the evaporation rates V of LiF/NaF/KF to be 1:1.3:12 at 1000 °C using Eq. (5). This indicates that the evaporation rate of KF was much faster than that of LiF and NaF in the early stages of the distillation process. This result was consistent with the experimental data in Table 3. In Run 9, when the evaporation ratio was 27%, the content of KF, 87.2 mol %, was much higher than that of LiF and NaF. As the distillation process continued, NaF and LiF started to evaporate. When the evaporation ratio reached 99% in Run 12, almost all the FLiNaK salt had evaporated, and the ratio of LiF/NaF/KF in the condensate was 45:12.2:42.8, almost equal to that of the original salt LiF–NaF–KF, 46.5:11.5:42 (mol %).

In an MSR system, the composition of the carrier salt should be precisely controlled, because the composition of the salt determines the melting point, viscosity, tolerance of the fuel or FP, etc. Table 3 shows that the composition of the condensed salt was not constant nor consistent with that of the fluoride salts used as the carrier salt or coolant when the evaporation ratios were different. A higher evaporation ratio ensured that the composition remained constant after the distillation process. For batch distillation, to recover a salt with the same composition as that of the carrier salt, the evaporation ratio should be as high as possible, as long as the DFs of the FPs are acceptable. In the present work, as the evaporation ratio ranged from 27 to 99%, the DF of Nd in the received salt ranged from 1.08×10^3 to 0.13×10^3 , which is higher than the value deemed acceptable for salt purification reported by ORNL (10^2). This indicated that the Nd content was approximately 50 ppm in the condensate at an evaporation ratio of 99%. In fact, in the actual nuclear fuel of the MSR, the total mass of the rare earth FPs is lower than the 0.1 wt% used in this study; thus, the content of rare earth elements in the received salt is less than 10 ppm, with a DF value of 100, and the condensate salt could be reused in the reactor.

4 Conclusion

A closed-chamber distillation system and a stair-step heating mode were developed to enhance the recovery performance and improve the recovery rate of FLiNaK melts. To determine the proper distillation temperature range, the temperature distribution of the system was first simulated using computational software. Compared with the simple heating process, the stair-step temperature mode proved to be effective and feasible for improving the salt recovery efficiency, with the recovery ratio reaching as high as 99%. Moreover, in this study, the method using the change curve of the pressure in the system was applied to determine the distillation process, especially the endpoint, and the distillation rate was calculated to be $0.015\text{--}0.027 \text{ g}\cdot\text{cm}^{-2} \text{ min}^{-1}$. Based on the recovery ratio of pure FLiNaK, the optimization process conditions were obtained and applied to the FLiNaK salts containing NdF₃. The separation efficiency was further estimated by changing the evaporation ratio; the DF of Nd was greater than 10^2 , with an evaporation ratio of 99%. The contents of the components, mainly the concentrations of LiF, NaF, and KF in the condensate salt, were determined, and the Nd content was approximately 75 ppm. The results showed that with a high evaporation ratio, the composition was almost equal to that of the original salt.

This research indicates that the closed-chamber distillation system can be used for FLiNaK distillation, using a stair-step heating method to achieve high recovery ratios; this method is also effective in the decontamination of FPs. Based on the ability of the equipment to prevent radioactive leakage and the high recovery ratio of the stair-step heating method, this study could provide a potential reference for pyro-processing of TMSR spent fuel.

Author contributions Qiang Dou and Qing-Nuan Li contributed to the study conception and design. Material preparation was performed by Jun-Xia Geng. Data collection was performed by

Yang Yang. Data analysis was performed by Yan Luo. The first draft of the manuscript was written by Hai-Ying Fu, and all authors commented on previous versions of the manuscript. All authors read and approved the final manuscript.

References

1. P. Baron, S.M. Cornet, E.D. Collins et al., A review of separation processes proposed for advanced fuel cycles based on technology readiness level assessments. *Prog. Nucl. Energy* **117**, 103091 (2019). <https://doi.org/10.1016/j.pnucene.2019.103091>
2. B.J. Riley, J. McFarlane, G.D. DelCul et al., Molten salt reactor waste and effluent management strategies: a review. *Nucl. Eng. Des.* **345**, 94–109 (2019). <https://doi.org/10.1016/j.nucengdes.2019.02.002>
3. M. Gowtham, V. Mahesh, J.C. Gomez-Vidalet et al., Assessment of a novel ternary eutectic chloride salt for next generation high-temperature sensible heat storage. *Energy Convers. Manag.* **167**, 156–164 (2018). <https://doi.org/10.1016/j.enconman.2018.04.100>
4. O. Beneš, R.J.M. Konings, Molten salt reactor fuel and coolant. In: Konings R.J.M., editor. *Comprehensive Nuclear Materials*, **3**, 359–389 (2012)
5. M.J. Kelly, Recovery of carrier salt by distillation, Reactor Chemistry Division Annual Progress Report, USAEC Report ORNL-3789, Oak Ridge National Laboratory, Jan. 31, 1965
6. J.R. Hightower, L.E. McNeese, Measurement of the relative volatilities of fluorides of Ce, La, Pr, Nd, Sm, Eu, Ba, Sr, Y and Zr in mixtures of LiF and BeF, ORNL-TM-2058, January 1968
7. S. Cantor, Molten-salt reactor program semiannual progress report, USAEC Report ORNL-4037, Oak Ridge National Laboratory, August 31, 1966
8. J.R. Hightower, L.E. McNeese, Low-pressure distillation of molten fluoride mixtures: nonradioactive tests for the MSRE distillation experiment, USAEC Report ORNL-4434, Oak Ridge National Laboratory, January 1971
9. C.D. Scott, W.L. Carter, Preliminary design study of a continuous fluorination- vacuum distillation system for regeneration fuel and fertile streams in molten salt breeder reactor, USAEC Report ORNL-3791, Oak Ridge National Laboratory, January 1966
10. B.R. Westphal, J.C. Price, D. Vaden et al., Engineering-scale distillation of cadmium for actinide recovery. *J. Alloy. Compd.* **444–445**, 561–564 (2007). <https://doi.org/10.1016/j.jallcom.2007.02.072>
11. B.R. Westphal, K. Marsden, J.C. Price, Development of a ceramic-lined crucible for the separation of salt from uranium. *Metall. Mater. Trans.* **40A**, 2861–2866 (2009). <https://doi.org/10.1007/s11661-009-9957-3>
12. H.L. Lee, G.I. Park, J.W. Lee et al., Current status of pyroprocessing development at KAERI. *Sci. Technol. Nucl. Install.* (2013). <https://doi.org/10.1155/2013/343492>
13. H.C. Eun, Y.Z. Cho, S.M. Son et al., Recycling of LiCl–KCl eutectic based salt wastes containing radioactive rare earth oxychlorides or oxides. *J. Nucl. Mater.* **420**, 548–553 (2012). <https://doi.org/10.1016/j.jnucmat.2011.11.048>
14. H.C. Eun, H.C. Yang, Y.J. Cho et al., Separation of pure LiCl–KCl eutectic salt from a mixture of LiCl–KCl eutectic salt and rare-earth precipitates by vacuum distillation. *J. Nucl. Sci. Technol.* **44**, 1295–1300 (2007). <https://doi.org/10.1080/18811248.2007.9711374>
15. M. Iizuka, M. Akagi, T. Koyama, High-temperature distillation and consolidation of U–Zr cathode product from molten salt electrorefining of simulated metallic fuel. *J. Nucl. Mater.* **448**, 259–269 (2014). <https://doi.org/10.1016/j.jnucmat.2014.02.015>
16. R. Harris, W.G. Davenport, Vacuum distillation of liquid metals: part I. Theory and experimental study. *Metall. Trans. B* **13**, 581–588 (1982). <https://doi.org/10.1007/BF02650016>
17. A.S. Basin, A.B. Kaplun, A.B. Meshalkin et al., The LiCl–KCl binary system. *Russ. J. Inorg. Chem.* **53**, 1509–1511 (2008). <https://doi.org/10.1134/S003602360809026X>
18. L.X. Sun, Y.S. Niu, C.W. Hu et al., Influence of molten salt composition on the fluorination of UF₄. *J. Fluor. Chem.* **218**, 99–104 (2019). <https://doi.org/10.1016/j.jfluchem.2018.11.015>
19. J.H. Zhou, J.L. Tan, B. Sun et al., The protective performance of a molten salt frozen wall in the process of fluoride volatility of uranium. *Nucl. Sci. Tech.* **30**, 102 (2019). <https://doi.org/10.1007/s41365-019-0620-4>
20. H.Y. Fu, J.X. Geng, Y. Yang et al., Low pressure distillation technology of molten salt in spent fuel pyroprocessing field. *Nucl. Tech.* **41**, 010603 (2018). <https://doi.org/10.11889/j.0253-3219.2018.hjs.41.040001>. (in Chinese)
21. Y. Luo, J.X. Geng, H.Y. Fu et al., The evaporation behaviour of ThF₄ mixed of FLiNaK melt during low-pressure distillation. *J. Nucl. Mater.* **525**, 48–52 (2019). <https://doi.org/10.1016/j.jnucmat.2019.07.026>
22. Z.H. Wang, H.Y. Fu, Y. Yang et al., The evaporation behaviors of rare-earth-doped FLiNaK melts during low-pressure distillation. *J. Radioanal. Nucl. Chem.* **311**, 637–642 (2017). <https://doi.org/10.1007/s10967-016-5110-0>
23. W. Huang, L.F. Tian, C.F. She et al., Electrochemical behavior of europium (III)–europium (II) in LiF–NaF–KF molten salt. *Electrochim. Acta* **147**, 114–120 (2014). <https://doi.org/10.1016/j.electacta.2014.08.119>
24. H.C. Eun, Y.Z. Cho, T.K. Lee et al., An improvement study on the closed chamber distillation system for recovery of renewable salts from salt wastes containing radioactive rare earth compounds. *J. Radioanal. Nucl. Chem.* **295**, 345–350 (2013). <https://doi.org/10.1007/s10967-012-1856-1>
25. W.L. Carter, R.B. Lindauer, L.E. McNeese, Design of an engineering-scale, vacuum distillation experiment for molten-salt reactor fuel, ORNL-TM-2213, Nov. 1968
26. Q. Dou, H.Y. Fu, Y. Yang et al., Distillation behaviors of LiF salt under different pressures and evaporation temperatures. *J. Nucl. Radiochem.* **36**(6), 357–362 (2014). <https://doi.org/10.7538/hhx.2014.36.06.0357>. (in Chinese)
27. D. Noriler, A.A.C. Barros, M.R.W. Maciel et al., Simultaneous momentum, mass, and energy transfer analysis of a distillation sieve tray using CFD techniques: prediction of efficiencies. *Ind. Eng. Chem. Res.* **49**, 6599–6611 (2010). <https://doi.org/10.1016/j.cej.2013.03.046>
28. B. Sun, J.H. Zhou, Q. Dou et al., Numerical analysis and experimental research on heat transfer equilibrium state of molten salt frozen wall. *Nucl. Tech.* **41**, 060601 (2018). <https://doi.org/10.11889/j.0253-3219.2018.hjs.41.060601>. (in Chinese)
29. S. Dushman, J.M. Lafferty, *Scientific foundations of vacuum technique* 2nd ed. John Wiley and Sons, New York, NY 1–39 (1962)
30. Y.S. Choi, H.J. Park, L. Taihyeop, Evaporation properties of FLiNaK with plasma interaction. Joint Conference of the 9th international conference on open magnetic systems for plasma confinement, 2012 Aug; Tsukuba (Japan), *Trans. Fusion Sci. Technol.* **63**, 221–224 (2013). <https://doi.org/10.13182/FST13-A16910>